Statistical properties of bidimensional patterns generated from delayed and extended maps

Giovanni Giacomelli,[1,2] Stefano Lepri,[3] and Antonio Politi[2,4]
[1]*Istituto Tecnico Industriale Statale "Tullio Buzzi," Prato, Italy*
[2]*Istituto Nazionale di Ottica, I-50125 Firenze, Italy*
[3]*Dipartimento di Fisica, Universitá di Bologna, I-40127 Bologna, Italy*
[4]*Istituto Nazionale di Fisica Nucleare, Sezione di Firenze, Firenze, Italy*
(Received 2 May 1994)

The space-time chaotic patterns associated with a class of dynamical systems ranging from delayed to extended maps are investigated. All the systems are constructed in such a way that the corresponding two-dimensional (2D) representation is characterized by the same updating rule in the bulk. The main difference among them is the direction of the "time" axis in the plane. Despite the different causality relations among the various models, the resulting patterns are shown to be statistically equivalent. In particular, the Kolmogorov-Sinai entropy density assumes always the same value. Therefore, it can be considered as an absolute indicator, measuring the amount of disorder of a 2D pattern. The Kaplan-Yorke dimension density is instead rule dependent: this indicator alone cannot be used to quantify the degrees of freedom of a given pattern; one must further specify the direction of propagation in the plane.

PACS number(s): 05.45.+b, 42.50.Lc

It is well known that low-dimensional chaotic signals can be characterized by well defined statistical indicators such as fractal dimension, entropy, and Lyapunov exponents [1]. Moreover, embedding theorems guarantee that it is possible, at least in principle, to reconstruct the underlying attractor. Less developed is the characterization of complex two-dimensional (2D) patterns associated with the high-dimensional dynamics of both spatially extended [2] and delayed systems [3]. As a first step in this direction, densities of entropies and of dimensions have been successfully introduced [4], suggesting that a dynamical system can be seen as a collection of many independent subsystems. A further issue arising in the analysis of 2D patterns is the occurrence of propagation phenomena not only in time, but also along the spatial direction. Comoving [5] and specific [6] Lyapunov exponents have been introduced in this context to account for the spreading of localized perturbations. In this paper we proceed further by comparing the patterns generated by the same rule iterated along different directions.

In the first part, we focus on the fairly wide class of delayed maps introduced in [7], clarifying to what extent they can be considered as equivalent to the commonly used coupled map lattices (CMLs) [8]. This is done in two steps: first, the typical 2D representation of delayed systems is introduced; then, the resulting model is mapped to a CML with asymmetric coupling by rotating the spatiotemporal reference frame. However, the equivalence is only formal, since different causality relations are present in the two cases: some future events in the delayed map are indeed past events in the CML representation and vice versa. Nevertheless, a careful quantitative investigation of the resulting patterns (by measuring Lyapunov spectra, correlation functions, block entropies, and effective dimensions) reveals a perfect invariance, suggesting that the same bulk rule is sufficient to guarantee a statistical equivalence.

In the second part, we introduce a more general class of dynamical systems which are intermediate between the delayed map and the CML. They correspond to generating a pattern by moving along different "time" directions in the plane. The determination of the Lyapunov spectrum in this family of models confirms that the Kolmogorov-Sinai entropy density is independent of the way the pattern is generated. Therefore, it is an absolute indicator of the disorder present in the reference pattern. Conversely, the fractal dimension, as computed from the Kaplan-Yorke formula, depends on the specific direction. Thus we cannot attribute a number of effective degrees of freedom to a given pattern: one must further specify the direction followed in either reading or generating the pattern itself. On the one hand, this result is somehow unexpected since the dimension is a static quantity referring to the invariant measure. On the other hand, the dependence of the dimension on the orientation can be seen as a measure of the anisotropy present in the pattern.

The most general updating rule for a discrete-time delayed system is

$$x_{n+1}=F(x_n,x_{n+1-T}) , \tag{1}$$

where the delay T represents also the phase-space dimension and F is a nonlinear mapping function from a given square $I\times I$ into the interval I. Such a mapping can be seen as the discretization of a differential equation of the type $\dot{x}(t)=g(x(t),x(t-\tau))$. Upon rewriting the time variable as

$$n=s+tT , \tag{2}$$

where t is the integer part of n/T, each label n can be identified by the space- and timelike variables s and t, respectively. By following this convention, the one-dimensional sequence of data is rearranged as a two-dimensional pattern. Accordingly, the evolution equa-

tion (1) can be interpreted as a mapping on a lattice of length T,

$$y_s^{t+1}=F(y_{s-1}^{t+1},y_s^t)\ ,\quad s=1,\ldots,T\ , \tag{3}$$

with the one-sided boundary condition $y_0^{t+1}=y_T^t$ [9]. At variance with usual coupled maps, where the lattice configuration is updated synchronously, in Eq. (3) we must proceed sequentially from $s=1$ to T. This is clearly a consequence of s not being a truly spatial variable. To recover the properties of the standard CML model we also rescale the time units by T [7]. One of the advantages of this formulation is that the long-range coupling, implicit in Eq. (1), can now be seen as a local interaction. The price that we have to pay is the increase of the state-space dimension: we pass from a zeroth-dimensional to a 1D extended system. This is a rather well known procedure [10].

Obviously, the exchange of delayed and local variables (DL transformation) in Eq. (1) leads, in general, to a different dynamics, unless the map F is DL invariant. However, if spatial and temporal variables also are exchanged (ST transformation), the initial bulk dynamical rule is recovered. Nevertheless, the boundary conditions are drastically different, so that it is not obvious whether the overall evolution is truly invariant under the composition of both transformations.

Let us now consider a last transformation that allows a more precise mapping of the dynamics (1) onto a CML model. By introducing a reference frame rotated by $\pi/4$ (see Fig. 1), we can label every point with the integers $i=s+t$ and $j=s-t$. After denoting the new variable as z_j^i, map (3) reads as

$$z_j^{i+1}=F(z_{j-1}^i,z_{j+1}^i)\ . \tag{4}$$

The lack of the coupling of z_j^{i+1} with z_j^i in Eq. (4) implies the existence of two distinct sublattices (open and full circles in Fig. 1) characterized by independent evolutions. Although Eq. (4) resembles the usual limit case $\varepsilon=\frac{1}{2}$ of a standard CML with diffusive coupling, here the left-right symmetry is, in general, lacking (unless F is DL invariant).

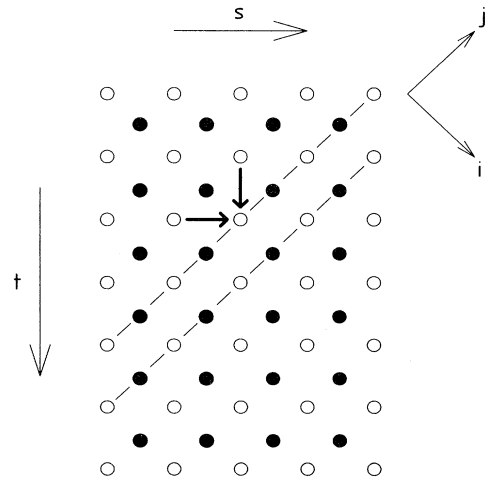

FIG. 1. Coupling scheme for the bidimensional representation of map (1). The map can be written as (4) in the tilted reference frame provided that we introduce an (independent) sublattice (full dots) and relabel the indices.

Since the updating procedure defined by Eq. (4) is synchronous, one might think that delayed maps can be naturally studied as usual CMLs [11]. However, there remains a crucial difference concerning the boundaries. In fact, we still have a one-sided condition, but now z_1^{i+1} (the chain is shifting rightward) is a function of all z_j^i $(i\le j\le i+T)$. Referring again to Fig. 1, it is immediately understood that, since y_1^s depends on y_T^{t-1}, it also depends implicitly on $(y_{T-1}^{t-1},y_T^{t-2})$. By repeating the same considerations, we have that $y_1^t=G(y_1^{t-1},y_2^{t-2},\ldots,y_T^{t-T})$, where G is some complicated function obtained by the proper compositions of F. The consequence of such a condition can by no means be considered as a "surface" effect; we are rather in the presence of a global nondemocratic coupling.

Let us specialize our analysis to the case [7]

$$x_{n+1}=(1-\varepsilon)f_1(x_n)+\varepsilon f_2(x_{n+1-T})\ , \tag{5}$$

where f_1 and f_2 are two maps of the unit interval and $0\le\varepsilon\le1$ gauges the relative weight of the delayed coupling with respect to the instantaneous one. The previous considerations lead to following three different maps:

$$y_s^{t+1}=(1-\varepsilon)f_1(y_{s-1}^{t+1})+\varepsilon f_2(y_s^t)\ \ \text{(model } A)\ , \tag{6}$$

$$y_s^{t+1}=(1-\varepsilon)f_1(y_s^t)+\varepsilon f_2(y_{s-1}^{t+1})\ \ \text{(model } B)\ , \tag{7}$$

$$z_j^{i+1}=(1-\varepsilon)f_1(z_{j-1}^i)+\varepsilon f_2(z_{j+1}^i)\ \ \text{(model } C)\ . \tag{8}$$

Model A is nothing but the bidimensional version of Eq. (5); model B is its DL transform; model C is the CML version corresponding to Eq. (4) with periodic boundary conditions assumed.

Since we want to compare the statistical properties of the chaotic patterns obtained by models $A-C$, let us begin with a case susceptible of analytic treatment, i.e., we choose f_1 and f_2 as two distinct Bernoulli shifts $f_1(x)=ax \bmod(1)$, and $f_2(x)=bx \bmod(1)$, with a and b being two positive constants. In Ref. [7] it was demonstrated that, for T large enough, the Lyapunov spectrum of model A is made of an "anomalous" (i.e., proportional to the delay) component

$$\lambda_A^{an}=T\ln[a(1-\varepsilon)]\ , \tag{9}$$

present only if $\lambda_A^{an}>0$, i.e., for $\varepsilon<(a-1)/a$, and of a continuous component

$$\lambda_A(\xi)=\frac{1}{2}\ln\left[\frac{b^2\varepsilon^2}{1+a^2(1-\varepsilon)^2-2a(1-\varepsilon)\cos\pi\xi}\right]\ , \tag{10}$$

where the index ξ $(0\le\xi\le1)$ is the integrated density of Lyapunov exponents. The spectrum λ_B of model B is obtained by simply exchanging a and b in (9) and (10).

Finally, the Lyapunov spectrum of map C can be easily calculated [12] by noticing that, due to the periodic

boundary conditions, the evolution matrix in tangent space commutes with the translation operator, yielding

$$\lambda_C(\xi)=\frac{1}{2}\ln[b^2(1-\varepsilon)^2+a\varepsilon^2+2ab\varepsilon(1-\varepsilon)\cos\pi\xi] . \quad (11)$$

The three spectra are, in general, different from one another.

From the knowledge of the Lyapunov spectrum, one can infer both the Kolmogorov-Sinai entropy and the dimension of the attractor. From the Pesin relation we can evaluate the entropy density K as the sum of all the positive exponents divided by T. In the thermodynamic limit we have

$$K_{A,B}=\lambda^{an}_{A,B}+\int\lambda_{A,B}(\xi)d\xi , \quad (12)$$

$$K_C=\int\lambda_C(\xi)d\xi , \quad (13)$$

where the integrals are extended to the positive part of the spectrum. Although an analytic expression of the entropy is to our knowledge not available, the numerical integration of Eqs. (12) reveals that $K_A=K_B=K_C$ for every value of the coupling parameter.

The Lyapunov dimension density D_{KY} of the attractor can be implicitly evaluated by means of the Kaplan-Yorke formula

$$\int_0^{D_{\mathrm{KY}}}\lambda(\xi)d\xi=0 . \quad (14)$$

The computation of D_{KY} in the three models shows that the dimension is different for the three maps.

To test the generality of these results we have performed numerical simulations in the case of f_2 being the logistic map $[f_2(x)=4x(1-x)]$ and f_1 the Bernoulli shift with slope a. The three models are again characterized by different Lyapunov spectra for all ε values, leading to different dimensions as reported in Fig. 2(a). Nevertheless, the same entropy density is always obtained as seen in Fig. 2(b). An intuitive explanation of this result is obtained by noticing that the amount of information contained in a given 2D pattern is the sum of a bulk contribution plus the incoming flux through the boundaries. In the thermodynamic limit, the latter contribution is asymptotically negligible, as it increases only with the number of sites along the perimeter. By recalling that the dynamical equations are equivalent in the three models, we can conclude that the Kolmogorov-Sinai entropy density is independent of the boundary conditions. On the other hand, the dimension seems to be strongly affected; it is therefore important to clarify to what extent the three spatiotemporal patterns are equivalent to each other.

To this aim we have computed several statistical indicators, starting from the spatiotemporal autocorrelation function

$$C^t_s=\frac{\langle x^{t'}_{s'}x^{t'-t}_{s'-s}\rangle-\langle x\rangle^2}{\langle x^2\rangle-\langle x\rangle^2} . \quad (15)$$

The results for model C is reported in Fig. 3(a). The other two models exhibit the same structure apart from either the expected reflection or rotation. A more quantitative comparison is produced in Fig. 3(b), where the correlation function is plotted along equivalent axes (spatial axis for model A, time axis in model B, and bisectrix in model C). The three curves are practically indistinguishable confirming the equivalence of the patterns.

In order to reveal more subtle correlations we have suitably encoded the data to perform a standard information theoretic study. The procedure simplifies if $f_1=f_2$, since in this case the DL transformation simply amounts to an exchange of ε with $1-\varepsilon$. The usual encoding procedure corresponds to associating 0 to values of the variable less than $\frac{1}{2}$ and 1 otherwise. We have then numerically estimated the probability $P_i^{(N\times M)}$ for any block i of $N\times M$ symbols to appear in the pattern, for $f_1=f_2=4x(1-x)$. The same probability is found for the corresponding blocks (obtained, for example, by exchanging s with the t axis in passing from model A to B). This equivalence extends the above mentioned coincidence of the Kolmogorov-Sinai entropy of the three processes to the fluctuations of this quantity.

The above results reveal increasing evidence that the patterns produced by the three processes are equivalent to each other. The only exception seems to be represent-

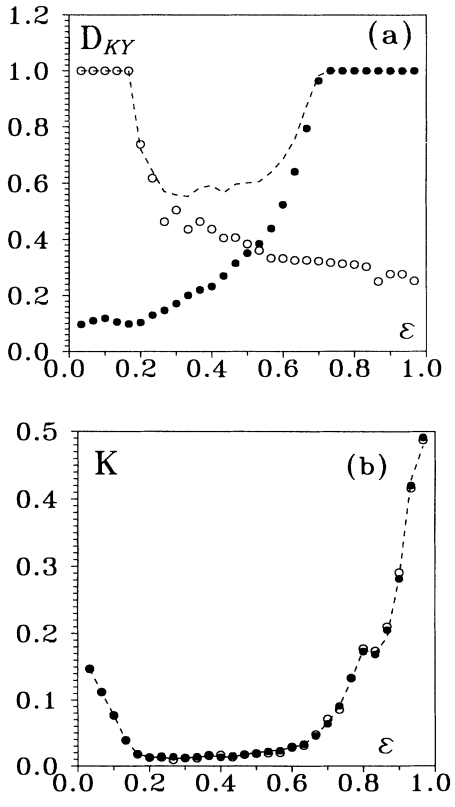

FIG. 2. (a) Kaplan-Yorke dimension density and (b) Kolmogorov-Sinai entropy density versus the coupling parameter for models A (full dots), B (open dots), and C (dashed line) with $f_1(x)=1.2x \bmod(1)$, $f_2(x)=4x(1-x)$, and $T=80$.

ed by the Lyapunov spectra (and, in turn, by the Kaplan-Yorke dimension) which are different in the three models. However, this diversity can be understood by noticing that Lyapunov exponents, as well as correlation functions, refer to a specific space-time direction. Therefore, one should more properly compare the usual "temporal" Lyapunov spectrum of model A with the "spatial" one [13] of model B.

The evidence that the dimension cannot be considered, at variance with the entropy, as an absolute quantity characterizing a given pattern may appear somehow unusual. We then investigated directly the fractal properties of the invariant measure by means of the nearest-neighbor algorithm [14]. More precisely, we computed the effective dimension

$$D_e(N) = -\left[\frac{d\langle \ln\delta(\mathbf{P},E,N,r)\rangle}{d\ln N}\right]^{-1}, \tag{16}$$

where $\mathbf{P}$ is a reference point, E is the embedding dimension, $\delta(\mathbf{P},E,N,r)$ is the distance of $\mathbf{P}$ from its rth nearest neighbor among N randomly chosen points, and $\langle\ \rangle$ denotes the average over the set of reference points. We performed several dimension estimates for an embedding dimension $E=10$ and for the tenth neighbor (different choices give qualitatively similar results). In Fig. 4(a), three effective dimensions are compared: both diamonds and open dots refer to spacelike vectors $(y_s^t, y_{s+1}^t, \ldots, y_{s+E-1}^t)$ for $\varepsilon=0.1$, but $T=E=10$ and 100, respectively, in the two cases. Full dots refer to timelike vectors $(y_s^t, y_s^{t+1}, \ldots, y_s^{t+E-1})$ for $\varepsilon=0.9$. Several comments are in order. First of all, an embedding dimension E equal to T is, by definition, sufficient to reconstruct the attractor topology and dimension (incidentally, the saturation value is close to the asymptotic value predicted by Kaplan-Yorke formula). The curve obtained for $T \gg E$ does not reveal any saturation. In fact, this case corresponds to projecting down a high-dimensional attractor onto an E-dimensional space, in complete analogy to what already observed in CMLs [15]. Much more interesting is the good overlap between open and full dots: it expresses once more the invariance of the dynamics under DL ($\varepsilon \to 1-\varepsilon$) plus ST (spacelike $\to$ timelike vectors) transformations. Indeed, because of the open boundary conditions implicitly assumed along the time axis, the measure associated with timelike vec-

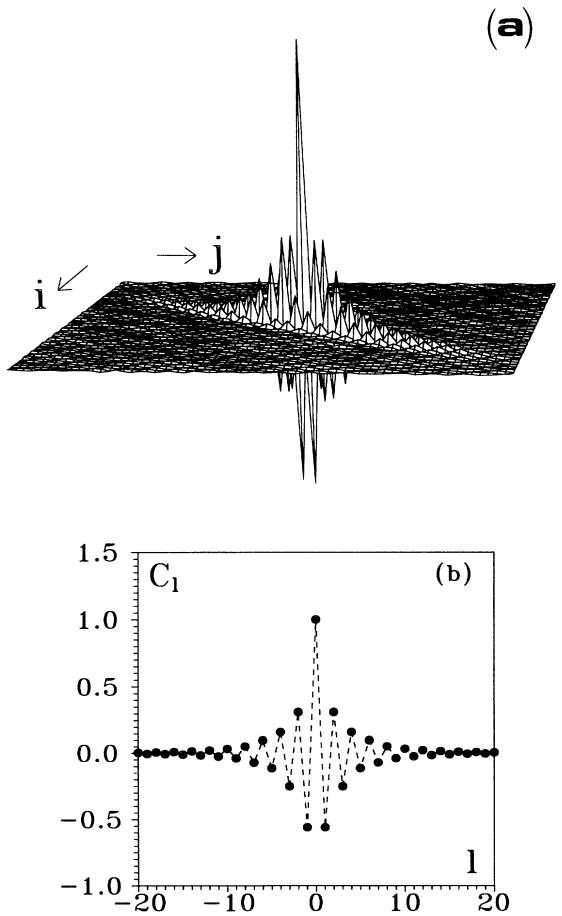

FIG. 3. (a) Bidimensional correlation function for model C and (b) its section along equivalent axis for models A, B, and C, with $f_1(x)=f_2(x)=4x(1-x)$, $\varepsilon=0.1$, and $T=1024$.

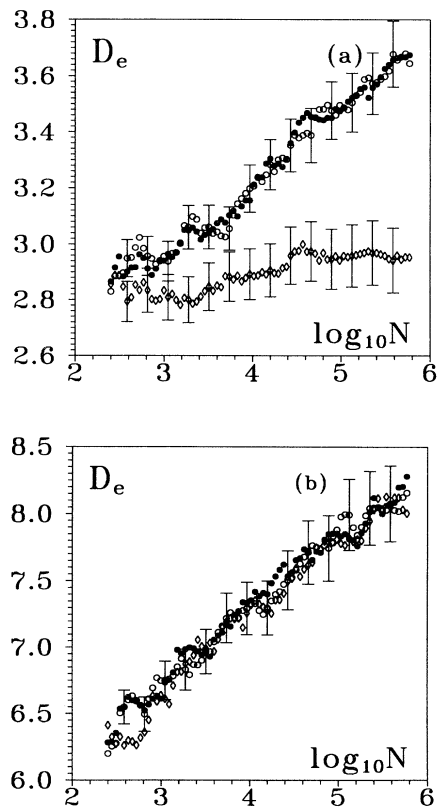

FIG. 4. Effective dimensions D_e measured with a nearest-neighbor algorithm (see text); in all cases 10^3 neighbors were considered.

tors is always the result of the projection of an infinite-dimensional attractor. Therefore, Fig. 4(a) confirms that statistically the same pattern is generated by using the same bulk rule, in spite of the strikingly different boundary conditions. The data plotted in Fig. 4(b) refer to the symmetric case, where space and time axes are exchanged. The agreement among the three curves is a consequence of the higher Kaplan-Yorke dimension. Already for $T=10$, a much larger number of points is needed to reach the same resolution and to observe the saturation to the expected value. The main result of the simulations reported in Fig. 4 is the difference between the curves in panel (a) with those in panel (b), i.e., the dependence of the dimension on the orientation of the time axis. The same pattern, imagined as being generated along two orthogonal directions, reveals a different number of effective degrees of freedom. In order to better understand this point, we have considered 1D lattices oriented in different ways in the plane. The dashed line in Fig. 5 refers to a tilted state with (average) slope $v=\frac{1}{2}$. At variance with Fig. 1, horizontal and vertical directions correspond to i and j axes (model C). One should remember also that only the dynamics on one of the two independent sublattices (open circles) is considered. Configurations with any slope can be obtained by suitably combining two different types of bonds: horizontal ones connecting site i with $i+2$ and $\pi/4$ tilted ones connecting neighboring sites. The extremum cases $v=\pm 1$ coincide with the delayed systems. After renumbering all the consecutive sites belonging to a given configuration, the mapping is rewritten in still another way which preserves the bulk evolution. The difference is again concentrated on the boundary conditions which are assumed to be periodic along the chain. By comparing a given state with the new one (solid line in Fig. 5), we find two different cases: either the variable y is updated from its past values in the neighboring sites or the newly updated y on the right neighbor is required. This means that synchronous and asynchronous updating rules are mixed up.

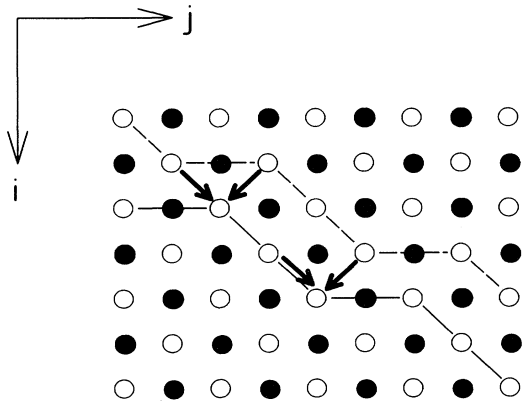

FIG. 5. Coupling scheme for the iteration of the map in a tilted reference frame with slope $v=\frac{1}{2}$.

The Lyapunov spectrum has been computed for several values of the velocity in the allowed v range $[-1,1]$ and for $\varepsilon=0.3$. We have then determined $K(v)$, $D_{KY}(v)$, and the dimension density D_u of the unstable manifold (i.e., the fraction of positive Lyapunov exponents). The entropy $K(v)$ turns out to be the same for all slopes v. This results extends the equality previously found in the extreme cases of models $A-C$ to a generic tilting. Let us remark that the independence of K on v is not trivial, since the number of positive Lyapunov exponents contributing to K exhibits notable fluctuations with v, as shown in Fig. 6(a) (full circles). The dimension D_{KY} also depends on v as seen in Fig. 6(a) (open circles). For $v=1$, -1, and 0, the known results for models A, B, and C, respectively, are recovered. The variation of D_{KY} with v is the key result of the simulations. It confirms that the dimension is not an absolute indicator to be associated with a given 2D pattern.

Finally, we have reported in Fig. 6(b) the maximum Lyapunov exponent versus v. The numerical data reveal a divergence for $v\to 1$. This result is connected with the

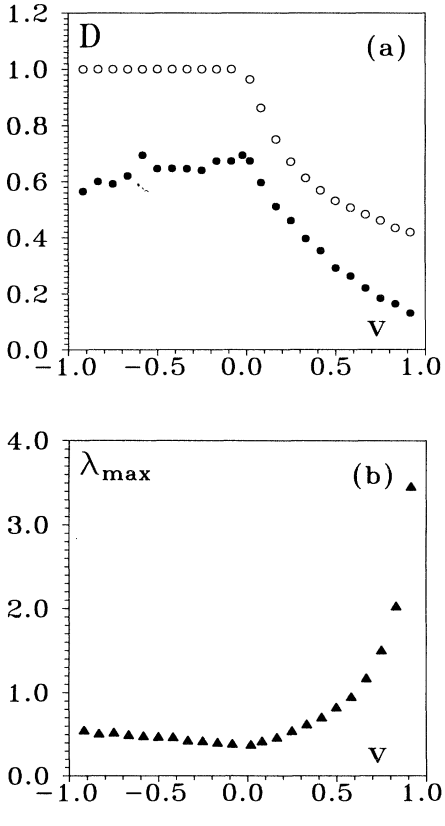

FIG. 6. (a) The Kaplan-Yorke dimension density D_{KY} (open dots) together with the fraction of positive exponents D_u (full dots) and (b) the maximum Lyapunov exponent λ_{max} versus v for $\varepsilon=0.3$ and $T=48$. The spectra have been computed iterating the map 2^8 times.

presence of an anomalous exponent which arises when the updating rule becomes entirely asynchronous.

The dependence of λ_{max} on v must not be confused with that of the maximal comoving Lyapunov exponent [5]. The former one is the growth rate of a statistically uniform perturbation distributed along the line $i=vj$. The latter one is the growth rate of an initially localized perturbation, observed along the world line $j=vi$. However, as the comoving Lyapunov exponents have been shown to be related to the class of specific exponents introduced in [6], we think that this new set of exponents is not independent of the previous ones. The study of possible connections is currently under investigation.

The reason why the slope v cannot exceed an absolute value of 1 is that in the CML representation, the maximum velocity of propagation of disturbances is just ± 1. Along a direction outside the light cone, the iteration of the dynamical rule requires inverting the local map; therefore, the evolution is expected to resemble the backward iteration of the lattice: the relevant invariant measure, rather than being a (strange) attractor, becomes a (strange) repellor. This is also the reason why the entropy as computed from the sum of the positive Lyapunov exponents along the spatial direction [6] can no longer be equal to the Kolmogorov-Sinai entropy: part of the local linear instability does not contribute to the information flow, but to the escape from the repellor [16].

Among the points not yet clarified in this work and the questions newly opened, we consider the possibility of extending the above concepts to continuous patterns as the most challenging one. We hope to be able to make some sensible progress in this direction, in the near future.

[1] D. Ruelle and J. P. Eckmann, Rev. Mod. Phys. **57**, 617 (1985).
[2] P. Manneville, *Dissipative Structures and Weak Turbulence* (Academic, San Diego, 1990).
[3] M. C. Mackey and L. Glass, Science **197**, 287 (1977); K. Ikeda and K. Matsumoto, J. Stat. Phys. **44**, 955 (1986).
[4] P. Grassberger, Phys. Scr. **40**, 346 (1989).
[5] R. J. Deissler and K. Kaneko, Phys. Lett. A **119**, 397 (1987).
[6] A. Politi and A. Torcini, Chaos **2**, 293 (1992).
[7] S. Lepri, G. Giacomelli, A. Politi, and F. T. Arecchi, Physica D **70**, 235 (1994).
[8] K. Kaneko, Prog. Theor. Phys. **72**, 980 (1984).
[9] The same kind of mapping arises in the numerical solution technique for first-order delay-differential equations; see J. D. Farmer, Physica D **4**, 366 (1982).
[10] T. Vogel, *Théorie des Systèmes Évolutifs* (Gauthier-Villars, Paris, 1965); F. T. Arecchi, G. Giacomelli, A. Lapucci, and R. Meucci, Phys. Rev. A **45**, 4225 (1992).
[11] The inverse analogy was noticed in F. H. Willeboordse, Int. J. Bif. Chaos **2**, 721 (1992).
[12] S. Isola, A. Politi, S. Ruffo, and A. Torcini, Phys. Lett. A **143**, 365 (1990).
[13] G. Giacomelli and A. Politi, Europhys. Lett. D **15**, 387 (1991).
[14] R. Badii and A. Politi, Phys. Rev. Lett. **52**, 1661 (1984).
[15] A. Politi and G. P. Puccioni, Physica D **58**, 384 (1992).
[16] T. Tèl, Phys. Rev. A **36**, 1502 (1987).